

Cite this: *Nanoscale*, 2021, **13**, 17101

Tunable Schottky barrier height of a Pt–CuO junction *via* a triboelectric nanogenerator

Jianping Meng, ^{a,b} Qi Li,^{a,c} Jing Huang^{a,c} and Zhou Li ^{*a,b,d}

Tuning Schottky barrier height is crucial to optimize the performance of Schottky junction devices. Here, we demonstrate that the Schottky barrier height can be tuned with the voltage from a triboelectric nanogenerator (TENG). Schottky barrier heights at both ends are increased after the treatment with the voltage generated by the TENG. The electric field generated by the impulse voltage of the TENG drives the diffusion of the ionized oxygen vacancy in a CuO nanowire, which induces the nonuniform distribution of the ionized oxygen vacancy. The positively charged oxygen vacancy accumulates at the contacted interface of Pt and the CuO nanowire, and it impels the conduction and valence bands to bend downwards. The Schottky barrier height is raised. A theoretical model based on the energy band diagram is proposed to explain this phenomenon. This method offers a simple and effective avenue to tune the Schottky barrier height. It opens up the possibility to develop a high-performance Schottky sensor by tuning the Schottky barrier height.

Received 22nd July 2021,
Accepted 13th September 2021

DOI: 10.1039/d1nr04752c

rsc.li/nanoscale

Introduction

Schottky contact plays an important role in virtually all micro-electric fields. The Schottky barrier height at a metal–semiconductor interface controls the depletion width and the mechanism of carrier transport.^{1,2} Tuning the Schottky barrier height can optimize the performance of Schottky devices.^{3,4} By tuning the Schottky barrier height, the detection performance is significantly enhanced for photodetectors,^{5–7} gas sensors,^{8,9} biosensors,^{10–12} chemical sensors,¹³ strain sensors,¹⁴ and so on.

The piezotronic effect as a dynamic adjusting method of Schottky barrier height is an effective way for piezoelectric semiconductors (including ZnO, GaN, ZnS, CdS, and so on) once a stress is applied.^{15–17} Then, the transport process of the carrier is modulated at the interface/junction.¹⁸ The piezotronic effect has been utilized to develop a high-performance sensor based on the Schottky contact.¹⁶ The piezoelectric semiconductor with a nanowire structure allows large deformations before fracture compared with bulk materials. However, the

risk of fracture is increased after multiple deformations in the process of the experiment. Another dynamic adjusting method is the polarization of charged oxygen vacancies in ZnO nanowires (n-type) using a triboelectric nanogenerator (TENG) with the properties of high voltage and low current.^{19–21} The discovery that the Schottky barrier height of the Ag–ZnO junction is decreased after being treated with the TENG is noticeable.^{5,9,11,22} The change of the Schottky barrier height based on a p-type nanowire semiconductor after being treated with the TENG still needs to be investigated to understand this effect in depth. CuO nanowires have been known as p-type semiconductors that exhibit a narrow bandgap and other interesting properties.^{23,24} CuO nanowires are promising p-type semiconductors due to their easy fabrication, low cost, environmentally friendly nature, and easy preparation. Schottky junctions based on CuO nanowires are widely applied in the fields of photodetectors,^{25–27} gas detection,^{28,29} chemical sensors,³⁰ memristors,³¹ field-effect transistors,³² and so on.

In this work, we chose a CuO nanowire as a p-type semiconductor to prepare a device with the Schottky junction. The high voltage produced by the TENG is used to modulate the Schottky barrier height. The Schottky barrier height of Pt and the CuO nanowire is increased after treatment with the TENG. A theoretical model is proposed to explain this phenomenon. The discovery in this work is beneficial for understanding the interaction mechanism between the impulse voltage of the TENG and Schottky barrier height. It provides an avenue to develop high-performance Schottky-contact sensors.

^aCAS Center for Excellence in Nanoscience, Beijing Key Laboratory of Micro-nano Energy and Sensor, Beijing Institute of Nanoenergy and Nanosystems, Chinese Academy of Sciences, Beijing, 101400, China. E-mail: zli@binn.cas.cn

^bSchool of Nanoscience and Technology, University of Chinese Academy of Sciences, Beijing 100049, P. R. China

^cCollege of Chemistry and Chemical Engineering, Guangxi University, Nanning, 530004, China

^dCenter on Nanoenergy Research, School of Physical Science and Technology, Guangxi University, Nanning 530004, P.R. China

Experimental

Materials preparation and characterization

CuO nanowires were synthesized by heating a copper substrate in air according to the protocol of Jiang *et al.*³³ The surface morphology of the CuO nanowire was obtained with a scanning electron microscope (SEM, Hitachi SU8020). The X-ray diffraction (XRD) pattern was used to obtain information on the phase structure using an X-ray diffractometer (PANalytical X'Pert) with a Cu K α source ($\lambda = 0.154$ nm). The composition and microstructure of CuO nanowire were investigated using a transmission electron microscope (TEM, Tecnai G² F20) equipped with a high-angle angular-dark-field detector and X-ray energy-dispersive spectrometer systems.

Fabrication of the TENG and Schottky junction

A 4 mm acrylic plate served as a robust substrate. Aluminum foil and a Kapton membrane were chosen as friction layers to generate a high voltage. The size of the aluminum foil and Kapton film is 8 cm \times 8 cm. The Cu film with a thickness of 50 nm deposited on the back side of the Kapton film with a thickness of 100 μ m is used as the electrode. Copper electrodes with a spacing of 10 μ m were deposited on the substrate of amorphous SiO₂ by UV-lithography technology. CuO nanowires were ultrasonically dispersed in ethanol. They were aligned on the Cu electrode array by electric-field assisted assembly and alignment. A voltage of 12 V with a frequency of 50 kHz is generated by the signal generator (ArbStudio 1104) to produce an alternating electric field. The Pt electrode was deposited on both sides of the CuO nanowires by the focused ion beam technology (FIB, FEI Scios 2) to form Schottky contact.

Electrical measurements

The voltage of the TENG was measured with a Tektronix oscilloscope (Type: HD06104). The I - V curve ranging from -5 V to 5 V was recorded using a semiconductor characterization system (Keithley 4200-SCS).

Results and discussion

The CuO nanowire is synthesized by the vapor–solid method. It is grown by heating a copper grid in air. The copper grid used in transmission electron microscopy was cleaned in an aqueous 1.0 M HCl solution for ~ 20 s. Afterward, it was rinsed with distilled water repeatedly, followed by drying under a N₂ gas flow. The copper grid was heated for 10 h in a tube furnace with a temperature of 500 $^{\circ}$ C immediately (Fig. 1a–d). CuO nanowires with lengths ranging from 10 μ m to 30 μ m were obtained (Fig. 1e). The XRD pattern indicates that the CuO nanowires are composed of CuO and Cu₂O. When the copper grid is heated in air, the major product is Cu₂O. CuO is synthesized slowly through the oxidation of Cu₂O further. In this case, Cu₂O is the precursor to the formation of CuO. The for-

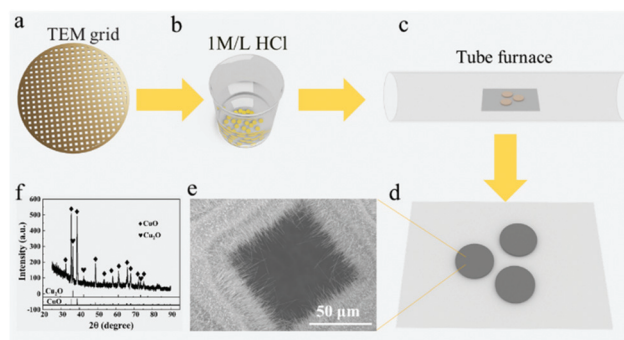


Fig. 1 Synthesis steps and characterization of CuO nanowires. (a–d) The synthesis process of the CuO nanowires. (e) SEM image of the CuO nanowires. (f) XRD pattern of the CuO nanowires.

mation of CuO vapor from Cu₂O is the rate-determining step.³³



The vapor pressure of CuO in the chamber is low due to the slow rate of the formation of CuO. It ensures a continuous growth mode and uniform diameter for the CuO nanowires. Additionally, the slow growth rate is beneficial for improving the crystallinity of the CuO nanowire.

The TEM method is utilized to characterize the morphology and microstructure further. The diameter of the prepared CuO nanowires is about 150 nm (Fig. 2a). The regular arrangement of atoms observed from a high-resolution TEM (HRTEM) image exhibits the nature of high crystallinity (Fig. 2b). The fluctuation in the arrangement of the atoms is due to slight stacking faults in the CuO nanowires. The interplanar distances measured from the HRTEM image are 2.496 \AA , 2.306 \AA , and 2.275 \AA , respectively, which are assigned to the panels of ($\bar{1}11$), (111), and (200) in the CuO nanowires. The two sets of diffraction spots are observed in the SAED image (Fig. 2c) con-

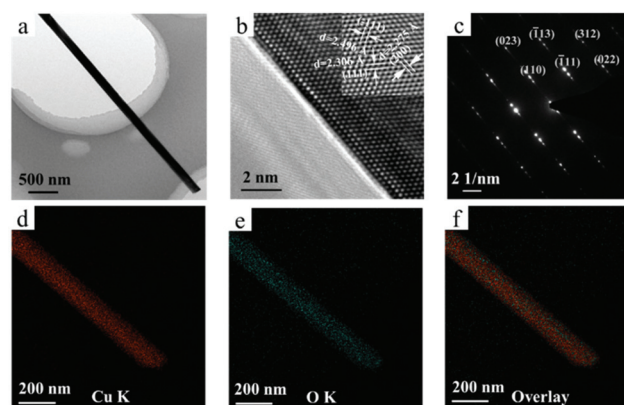


Fig. 2 Structural information of the CuO nanowire. (a–c) TEM, HRTEM, and SAED images of the CuO nanowire. (d–f) EDS element mapping of Cu and O.

firming the existence of stacking faults within the CuO nanowire. The calibration of diffraction spots corresponds to the diffraction of the lattice plane in CuO. The EDS spectrum of a single CuO nanowire shows red (Cu) and green (O) colors (Fig. 2e and f). The clear signal of Cu and O elements is further evidence of the CuO nanowire.

The voltage of the TENG after rectification is applied on a Pt–CuO–Pt Schottky diode (Fig. 3a). The corresponding equivalent circuit is shown in Fig. 3b. R_{nw} is the resistance of the nanowire. R_{sh1} and R_{sh2} are the shunt resistances associated with the two Schottky barriers.^{34,35} The output voltage of the TENG after rectification is about 180 V with a frequency of 1 Hz (Fig. 3c). The device exhibits a non-linear I - V curve, which indicates that the Schottky junction is formed between Pt and the CuO nanowire at both ends (Fig. 3d). The almost symmetrical I - V curve infers the approaching Schottky barrier height. The inset image at the top of Fig. 3d is the SEM image of the Pt–CuO–Pt Schottky diode. The almost same Schottky barrier heights are formed owing to the homogeneous CuO nanowire and the stable FIB technology. According to the classic thermionic emission-diffusion theory ($V \gg 3kT/q \sim 77$ mV),^{36,37} the current of the Schottky diode can be determined using the following formula:

$$I_R = SA^*T^2 \exp\left(-\frac{\phi_{B0}}{kT}\right) \exp\left(\frac{\sqrt{q^7 N_D (V + V_{bi} - kT/q)} / (8\pi^2 \epsilon_s^3)}{kT}\right) \quad (1)$$

in which S is the contact area between the metal and semiconductor, A^* is the effective Richardson constant, whose value is $14.5 \text{ A cm}^{-2} \text{ K}^2$,³⁸ T is the absolute temperature, ϕ_{B0} is the Schottky barrier height, k is the Boltzmann constant, q is the unit electronic charge, N_D is the doping concentration, V is

the applied voltage, V_{bi} is the built-in potential, and ϵ_s is the permittivity of CuO. The Schottky barrier height is obtained by plotting the curve of $\ln(I)$ and $V^{1/4}$. Schottky barrier heights of the drain and source are 0.56 and 0.55 eV after calculation. The inset image at the bottom of Fig. 3d is a schematic of the Pt–CuO–Pt Schottky diode.

The I - V curves before and after TENG treatment are shown in Fig. 4a. The current of the Pt–CuO–Pt Schottky diode is decreased after TENG treatment, and additionally, the decrease amount is enhanced with the increase of treatment times. The Schottky barrier heights of the source and drain are raised from 0.55 and 0.56 eV to 0.59 and 0.60 eV (Fig. 4b). The Schottky barrier height increases monotonically by increasing times of TENG treatment. When Pt and the CuO nanowire are brought in contact, the Schottky barrier (hole barrier) is formed because of (i) the difference of the work function of Pt and the ionization energy of the CuO nanowire, and (ii) the surface state of the CuO nanowire (Fig. 4c). The conduction and valence bands bend downwards. The Schottky barrier height is increased after the treatment with the voltage from the TENG (Fig. 4d). It is well known that the native oxygen defect is generated inevitably during the synthetic process of CuO nanowires because of low formation energy.²⁶ It is shown as the black spheres in the atomic structure of CuO (Fig. 4c). Defects in the CuO nanowire create defect localized states. The interaction of the external electric field and localized state around the oxygen defect occurs once the electric field is

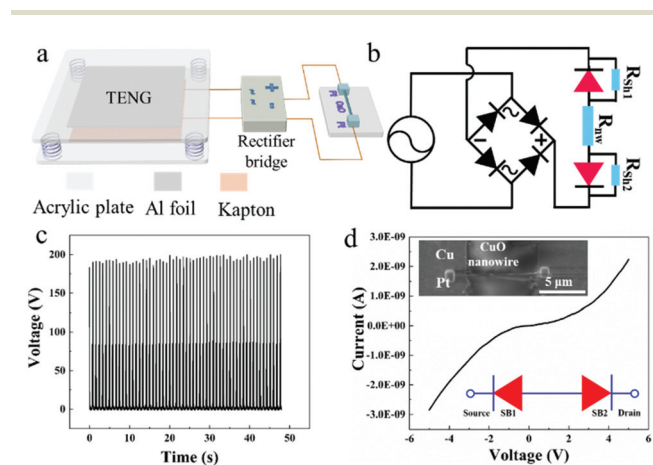


Fig. 3 Diagram of the experimental setup and basic performance of the TENG and Pt–CuO–Pt Schottky device. (a) Schematic illustration of the experimental setup. (b) equivalent circuit corresponding to figure a. (c) Open-circuit voltage of the TENG. (d) I - V curve of the Pt–CuO–Pt Schottky device; the inset on the top is the SEM image of Pt–CuO–Pt and the inset at the bottom is the schematic structure of the device.

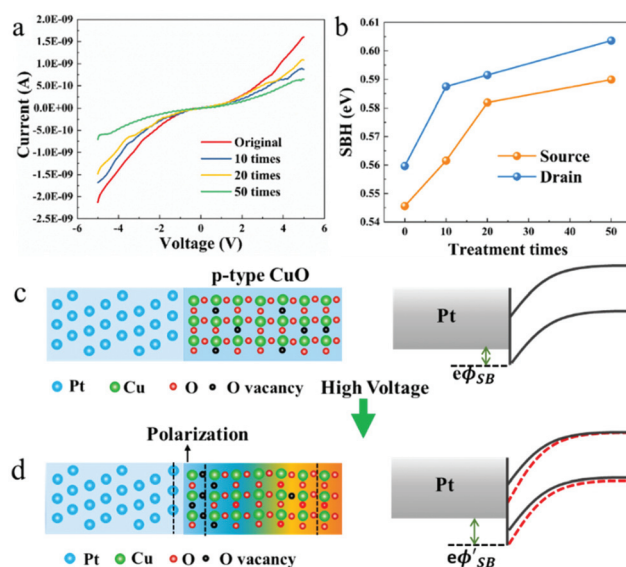


Fig. 4 Change of the Schottky barrier height and polarization model of the Pt and CuO (p-type) interface to Pt–CuO–Pt. (a) I - V curves of the Pt–CuO–Pt device with different times of TENG treatment. (b) The corresponding change of Schottky barrier height at the source and drain. (c) Schematic atomic structure of the Pt–CuO device, the band diagram of the Schottky contact Pt–CuO (p-type) interface at the initial state. (d) The oxygen vacancies are driven by the positive high voltage of the TENG, and they are accumulated at the junction around the interface.

applied. The electrical potential induced by the external electrical field will be proportionally and directly converted into energy gain in CuO nanowires associated with local lattice relaxations. The oxygen vacancy is charged under the stimulation of the electric field from the output voltage of the TENG. It converts into an ionized oxygen vacancy ($V_{\text{O}}^0 \rightarrow e + V_{\text{O}}^+$ or $V_{\text{O}}^+ \rightarrow e + V_{\text{O}}^{2+}$).^{39,40} Ionized oxygen vacancies are diffused toward the interface of Pt and the CuO nanowire. The ionized oxygen vacancy with positive charge accumulated at the interface.⁴¹ It acts as the positive “gate” voltage, which leads to the conduction and valence bands of CuO around the interface bending downwards simultaneously. The Schottky barrier height formed by Pt and the CuO nanowire is raised.

Conclusions

In summary, we investigate the influence of the impulse voltage of the TENG on the Schottky barrier height of Pt–CuO–Pt. First, the uniform CuO nanowires (~150 nm in diameter) with lengths ranging from 10 to 30 μm are synthesized by the vapor–solid method. The stacking fault is found in the CuO nanowire by HRTEM and SAED analyses. Then, the Schottky-contact device based on CuO nanowires and Pt is fabricated by electric-field assisted alignment and focused ion beam technology. The interaction of the output voltage from the TENG and CuO nanowire-based Schottky junction is investigated. The Schottky barrier height is raised after the treatment with the voltage of the TENG. A theoretical model based on the energy band diagram is proposed to explain the phenomenon of the change of Schottky barrier height. The oxygen vacancy is transferred into the ionized oxygen vacancy under the impact of the voltage from the TENG. The ionized oxygen vacancy is diffused toward the contact interface of Pt and the CuO nanowire, which leads to the increase of Schottky barrier height. This work is beneficial for understanding the tuning effect of Schottky barrier height in depth. This method opens up the possibility to develop a high-performance Schottky sensor by modulating Schottky barrier height.

Author contributions

Jianping Meng: Conceptualization, investigation, methodology, writing – original draft, data curation, validation, and funding acquisition. Qi Li: Investigation and data curation. Jing Huang: Investigation. Zhou Li: Supervision, resources, funding acquisition, and writing – review and editing. All authors: writing – review and editing.

Conflicts of interest

There are no conflicts to declare.

Acknowledgements

The authors are thankful for the support provided by the Beijing Natural Science Foundation (2214083, and JQ20038), the National Natural Science Foundation of China (52002027, T2125003, and 61875015), and the Youth Backbone Individual Project of Beijing Excellent Talents Training (Y9QNGG0501).

References

- 1 R. T. Tung, *Mater. Sci. Eng., R*, 2001, **35**, 1–138.
- 2 J. P. Meng and Z. Li, *Adv. Mater.*, 2020, **32**, 2000130.
- 3 R. Yu, S. Niu, C. Pan and Z. L. Wang, *Nano Energy*, 2015, **14**, 312–339.
- 4 C. F. Pan, J. Y. Zhai and Z. L. Wang, *Chem. Rev.*, 2019, **119**, 9303–9359.
- 5 H. Li, L. M. Zhao, J. P. Meng, C. F. Pan, Y. Zhang, Y. M. Zhang, Z. Liu, Y. Zou, Y. B. Fan, Z. L. Wang and Z. Li, *Nano Today*, 2020, **33**, 100873.
- 6 Z. Yang, M. Jiang, L. Guo, G. Hu, Y. Gu, J. Xi, Z. Huo, F. Li, S. Wang and C. Pan, *Nano Energy*, 2021, **85**, 105951.
- 7 F. Yang, M. L. Zheng, L. Zhao, J. M. Guo, B. Zhang, G. Q. Gu, G. Cheng and Z. L. Du, *Nano Energy*, 2019, **60**, 680–688.
- 8 N. Simiao, H. Youfan, W. Xiaonan, Z. Yusheng, Z. Fang, L. Long, W. Sihong and W. Z. Lin, *Adv. Mater.*, 2013, **25**, 3701–3706.
- 9 J. P. Meng, H. Li, L. M. Zhao, J. F. Lu, C. F. Pan, Y. Zhang and Z. Li, *Nano Lett.*, 2020, **20**, 4968–4974.
- 10 P. H. Yeh, Z. Li and Z. L. Wang, *Adv. Mater.*, 2009, **21**, 4975–4978.
- 11 L. M. Zhao, H. Li, J. P. Meng, A. C. Wang, P. C. Tan, Y. Zou, Z. Q. Yuan, J. F. Lu, C. F. Pan, Y. B. Fan, Y. M. Zhang, Y. Zhang, Z. L. Wang and Z. Li, *Adv. Funct. Mater.*, 2020, **30**, 1907999.
- 12 R. Yu, C. Pan, J. Chen, G. Zhu and Z. L. Wang, *Adv. Funct. Mater.*, 2013, **23**, 5868–5874.
- 13 C. Pan, R. Yu, S. Niu, G. Zhu and Z. L. Wang, *ACS Nano*, 2013, **7**, 1803–1810.
- 14 Z. Zhang, Q. L. Liao, X. H. Zhang, G. J. Zhang, P. F. Li, S. N. Lu, S. Liu and Y. Zhang, *Nanoscale*, 2015, **7**, 1796–1801.
- 15 Z. L. Wang, *J. Phys. Chem. Lett.*, 2010, **1**, 1388–1393.
- 16 Z. L. Wang and W. Z. Wu, *Natl. Sci. Rev.*, 2014, **1**, 62–90.
- 17 W. Z. Wu and Z. L. Wang, *Nat. Rev. Mater.*, 2016, **1**, 16031.
- 18 Z. L. Wang, W. Z. Wu and C. Falconi, *MRS Bull.*, 2018, **43**, 922–927.
- 19 H. F. Qin, G. Q. Gu, W. Y. Shang, H. C. Luo, W. H. Zhang, P. Cui, B. Zhang, J. M. Guo, G. Cheng and Z. L. Du, *Nano Energy*, 2020, **68**, 10432.
- 20 L. Zhao, K. Chen, F. Yang, M. L. Zheng, J. M. Guo, G. Q. Gu, B. Zhang, H. F. Qin, G. Cheng and Z. L. Du, *Nano Energy*, 2019, **62**, 38–45.

- 21 M. L. Zheng, F. Yang, J. M. Guo, L. Zhao, X. H. Jiang, G. Q. Gu, B. Zhang, P. Cui, G. Cheng and Z. L. Du, *Nano Energy*, 2020, **73**, 104808.
- 22 L. M. Zhao, H. Li, J. P. Meng, Y. Zhang, H. Q. Feng, Y. X. Wu and Z. Li, *Sci. Bull.*, 2021, **66**, 1409–1418.
- 23 A. Tombak, M. Benhaliliba, Y. S. Ocak and T. Kilicoglu, *Results Phys.*, 2015, **5**, 314–321.
- 24 C. Florica, A. Costas, A. G. Boni, R. Negrea, L. Ion, N. Preda, L. Pintilie and I. Enculescu, *Appl. Phys. Lett.*, 2015, **106**, 223501.
- 25 P. Wang, X. H. Zhao and B. J. Li, *Opt. Express*, 2011, **19**, 11271–11279.
- 26 L. B. Luo, X. H. Wang, C. Xie, Z. J. Li, R. Lu, X. B. Yang and J. Lu, *Nanoscale Res. Lett.*, 2014, **9**, 1–8.
- 27 T.-Y. Wei, C.-T. Huang, B. J. Hansen, Y.-F. Lin, L.-J. Chen, S.-Y. Lu and Z. L. Wang, *Appl. Phys. Lett.*, 2010, **96**, 013508.
- 28 S. Steinhauer, E. Brunet, T. Maier, G. C. Mutinati, A. Kock, O. Freudenberg, C. Gspan, W. Grogger, A. Neuhold and R. Resel, *Sens. Actuators, B*, 2013, **187**, 50–57.
- 29 L. Liao, Z. Zhang, B. Yan, Z. Zheng, Q. L. Bao, T. Wu, C. M. Li, Z. X. Shen, J. X. Zhang, H. Gong, J. C. Li and T. Yu, *Nanotechnology*, 2009, **20**, 085203.
- 30 D. D. Li, J. Hu, R. Q. Wu and J. G. Lu, *Nanotechnology*, 2010, **21**, 485502.
- 31 Z. Fan, X. D. Fan, A. Li and L. X. Dong, *Nanoscale*, 2013, **5**, 12310–12315.
- 32 B. J. Hansen, N. Kouklin, G. H. Lu, I. K. Lin, J. H. Chen and X. Zhang, *J. Phys. Chem. C*, 2010, **114**, 2440–2447.
- 33 X. C. Jiang, T. Herricks and Y. N. Xia, *Nano Lett.*, 2002, **2**, 1333–1338.
- 34 Z. Y. Zhang, K. Yao, Y. Liu, C. H. Jin, X. L. Liang, Q. Chen and L. M. Peng, *Adv. Funct. Mater.*, 2007, **17**, 2478–2489.
- 35 Y. Liu, Z. Y. Zhang, Y. F. Hu, C. H. Jin and L. M. Peng, *J. Nanosci. Nanotechnol.*, 2008, **8**, 252–258.
- 36 K. K. Ng and S. M. Sze, *Physics of Semiconductor Devices*, New York, NY, 1981.
- 37 J. Zhou, Y. D. Gu, P. Fei, W. J. Mai, Y. F. Gao, R. S. Yang, G. Bao and Z. L. Wang, *Nano Lett.*, 2008, **8**, 3035–3040.
- 38 R. Jana, S. Sil, A. Dey, J. Datta and P. P. Ray, *AIP Adv.*, 2018, **8**, 125104.
- 39 S. Lany and A. Zunger, *Phys. Rev. B: Condens. Matter Mater. Phys.*, 2005, **72**, 035215.
- 40 B. L. Huang, M. Z. Sun and D. F. Peng, *Nano Energy*, 2018, **47**, 150–171.
- 41 Y. Ding, Y. Liu, S. M. Niu, W. Z. Wu and Z. L. Wang, *J. Appl. Phys.*, 2014, **116**, 154304.